Calibrating Semi-analytic Models of the First Galaxies with Hydrodynamical Simulations to Enable Computationally Efficient Observational Predictions

Ryan Hazlett[1], Mihir Kulkarni[1], Eli Visbal[1], John H. Wise[2]

[1]Ritter Astrophysical Research Center, Department of Physics and Astronomy, University of Toledo
[2]Center for Relativistic Astrophysics, Georgia Institute of Technology

Introduction

- Understanding the properties of the first stars and galaxies has become critical for interpreting future observations with JWST.
- Cosmological hydrodynamical simulations accurately model the relevant physics, but due to large computational cost, cannot span the redshifts, volumes, and parameter space (e.g., Population III initial mass function) necessary to connect with observations.
- Semi-analytic models (SAMs) are computationally fast, but typically have many free parameters which limit their predictive power.
- Our new approach combines the strengths of these theoretical techniques by calibrating a semi-analytic model (Visbal et al. 2020) to the *Renaissance* simulations (state-of-the-art hydrodynamical cosmological simulations of the first stars and galaxies).

A Two-Phase Model for Metal-Enriched Star Formation

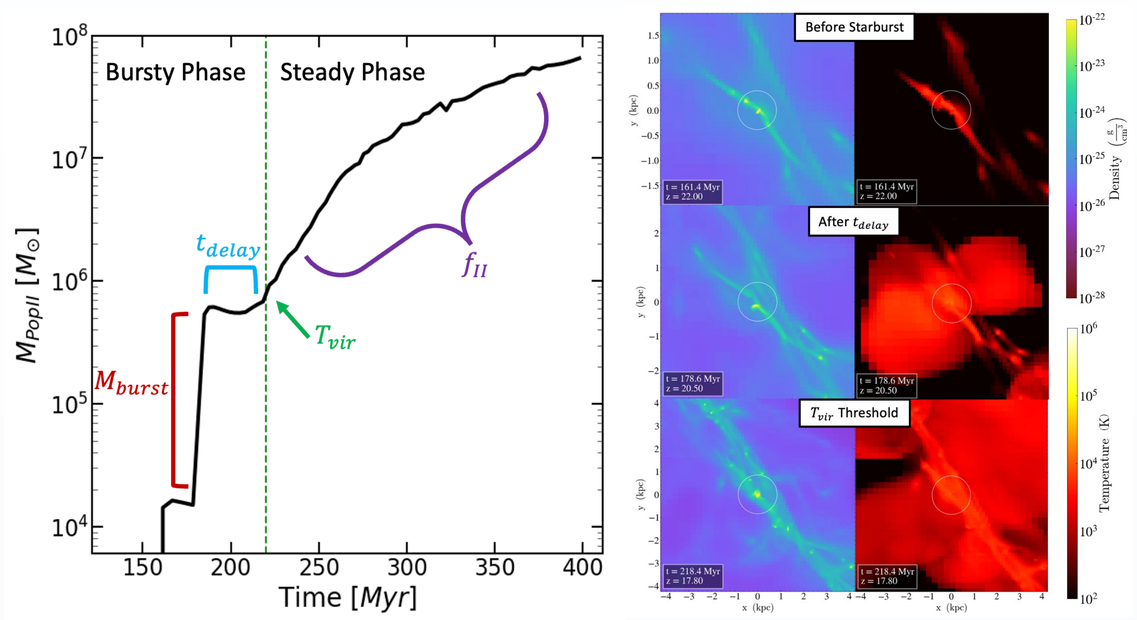

Figure 1. (Left) Metal-enriched star formation history for a single Renaissance halo. M_{PopII} is the total mass of Pop II stars formed in the halo. The burst stellar mass, quiescent period, threshold temperature, and star formation efficiency are labeled M_{burst}, t_{delay}, T_{vir}, and f_{II} respectively. **(Right)** Density and temperature projections 10x the halo virial radius shown as a white circle.

- Bursty Phase: Begins after the death of Pop III stars and dispersal of their metals into the ISM. Pop II stars form in a rapid starburst and expels gas from the gravitational potential well. Star formation then enters a quiescent period as gas falls back into the halo. A halo can experience multiple bursts and quiescent periods
- Steady Phase: Once the halo reaches a threshold, gas heating due to reionization no longer significantly suppresses star formation (Dijkstra et al. 2004). Subsequent star formation forms orders of magnitude more of Pop II.
- The division of metal-enriched star formation into bursty and steady phases is the foundation for our calibration to *Renaissance* and implementation in our semi-analytic model.

Calibration to Renaissance

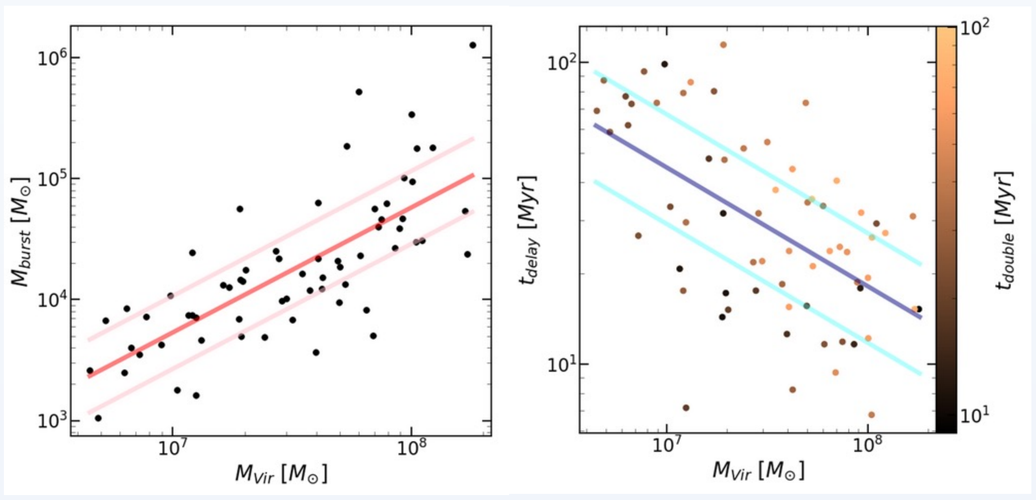

Figure 2. (Left) Metal-enriched starburst masses from sample of *Renaissance* halos. Power law fit (red) and 1-sigma confidence intervals (pink). **(Right)** Quiescent times from sample . Power law fit (blue) and 1-sigma confidence intervals (cyan). Color bar shows viral mass doubling time of halo.

- Gathered a sample of 27 dark matter and stellar mass histories illustrative of typical metal enriched star formation in *Renaissance*. We visually identify when Pop II bursts and quiescent periods occur along with the start of steady star formation.
- M_{burst} and t_{delay} are strongly correlated with virial mass. Properties like redshift, time since last Pop III SN, viral mass doubling time, etc., show weak dependence.

Steady Phase Coupled Differential Equations

$$\dot{m}_\star = \frac{\epsilon_{ff}}{t_{ff}} m_g$$

$$\dot{m}_g = \dot{m}_{acc,g} - \dot{m}_\star - \eta \dot{m}_\star$$

- Assign burst masses and quiescent times to halos by sampling from power law fits with some random scatter. We find a threshold near $T_{vir} = 1.76\times10^4 K$ for the transition to the steady phase in most sample star formation histories.
- We calculate best fit star formation efficiencies ϵ_{ff} that satisfy the above equations from Furlanetto and Mirocha (2022) for every SF history in our sample. We adopt a SN ejection efficiency η consistent with Sassano et al. (2021).
- SF efficiencies follow a log-normal distribution which is drawn from by our semi-analytic model during the steady phase.

Ionized HII Bubble Comparison

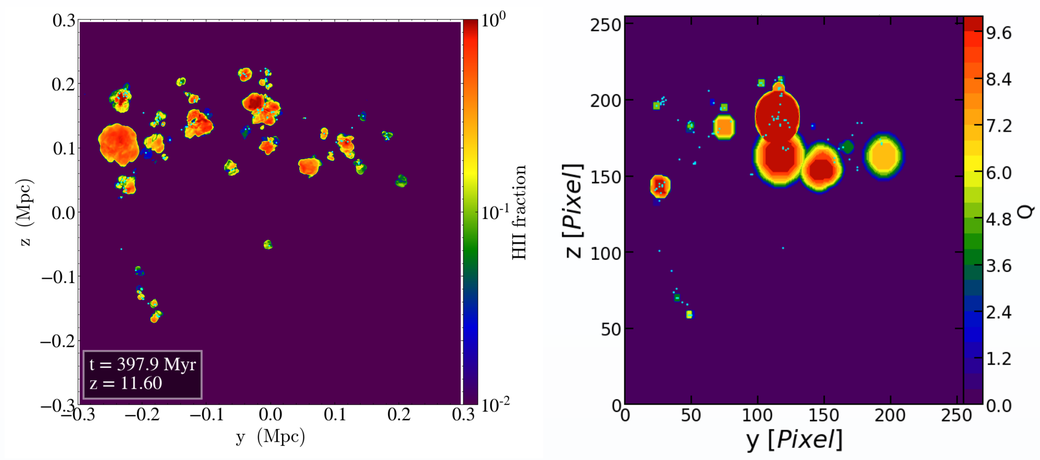

Figure 3. Comparison of ionized HII bubbles for a 20 kpc slice at z=11.6. Small cyan dots are halos with Pop II and Pop III stars. **(Left)** HII fraction for the slice in *Renaissance*. **(Right)** The same slice for the 256^3-resolution grid in our semi-analytic model used to calculate HII regions. Q is set to 1 for a single fully ionized grid.

- Our model is based on dark matter halo merger trees from cosmological N-body simulations (including 3D spatial positions), and incorporates feedback from Lyman-Werner radiation, growth of HII regions in the intergalactic medium, and metal enrichment from supernovae winds.
- We reproduce the IGM properties of *Renaissance* reasonably well using fiducial parameters from Visbal et al. (2020). We expect the agreement to further improve with calibrations of the escape fractions, inclusion of recombination, and no longer assuming a uniform IGM.

Can a SAM Reproduce Star Formation in Renaissance?

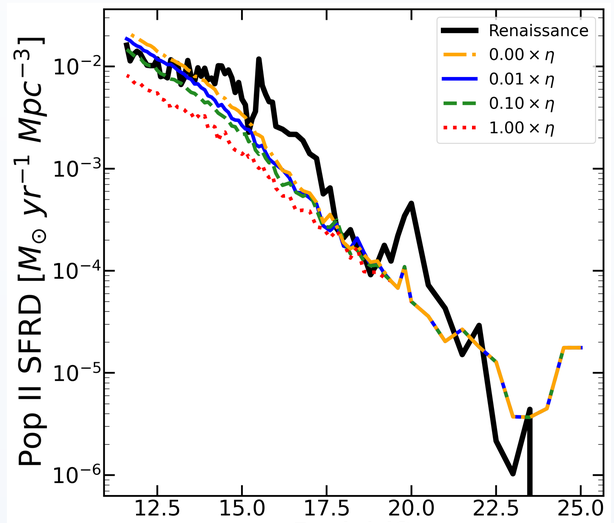

Figure 4. Each curve is the average Pop II star formation rate density from 10 simulations of our semi-analytic model. We vary SN ejection efficiency by factors of 10 and compare with *Renaissance*.

- Our calibrated semi-analytic model produces Pop II star formation consistent with *Renaissance*.
- Metal-enriched star formation histories for individual halos are well reproduced by the best fit values and random scatter for M_{burst}, t_{delay}, T_{vir}, and f_{II}.
- We find that weaker SN feedback is the best fit for the *Renaissance* Normal region.

Conclusions

- Our model reproduces the metal-enriched star formation and IGM properties of *Renaissance* at a fraction of the computational cost (tens of CPU hours compared to 8 million CPU hours).
- This allows us to expand to larger volumes, extend to lower redshifts, and span larger parameter spaces than previously possible.
- In future work, we will make a variety of observational predictions (late Pop III star formation, supernovae rates, stellar archaeology, etc.) using our calibrated model.

References and Acknowledgments

Dijkstra, M., Haiman, Z., Rees, M. J., & Weinberg, D. H. 2004, ApJ, 601, 666
Furlanetto S. R., Mirocha J., 2022, MNRAS, 511, 3895
Sassano F., Schneider R., Valiante R., Inayoshi K., Chon S., Omukai K., Mayer L., Capelo P. R., 2021, MNRAS, 506, 613
Visbal E., Bryan G. L., Haiman Z., 2020, ApJ, 897, 95
Xu, H., Wise, J. H., & Norman, M. L. 2013, ApJ, 773, 83

Ohio Supercomputer Center
An OH·TECH Consortium Member

This work is supported in part by NSF grant AST-2009309 and NASA ATP grant 80NSSC22K0629. All numerical simulations were carried out at the Ohio Supercomputer Center (OSC).